Scaling and modeling in the analysis of dispersive relaxation of ionic materials

J. Ross Macdonald[a]
Department of Physics and Astronomy, University of North Carolina,
Chapel Hill, North Carolina 27599-3255

Problems with scaling of conductive-system experimental $M''_{dat}(\omega)$ and $\sigma'_{dat}(\omega)$ data are considered and resolved by dispersive-relaxation-model fitting and comparison. Scaling is attempted for both synthetic and experimental $M''(\omega)$ data sets. A crucial element in all experimental frequency-response data is the influence of the high-frequency-limiting dipolar-and-vibronic dielectric constant $\varepsilon_{D\infty}$, often designated ε_∞, and not related to ionic transport. It is shown that $\varepsilon_{D\infty}$ precludes scaling of $M''_{dat}(\omega)$ for ionic materials when the mobile-charge concentration varies. When the effects of $\varepsilon_{D\infty}$ are properly removed from the data, however, such scaling is viable. Only the $\sigma'(\omega)$ and $\varepsilon''(\omega)$ parts of immittance response are uninfluenced by $\varepsilon_{D\infty}$. Thus, scaling is possible for experimental $\sigma'(\omega)$ data sets under concentration variation if the shape parameter of a well-fitting model remains constant and if any parts of the response not associated with bulk ionic transport are eliminated. Comparison between the predictions of the original-modulus-formalism (OMF) response model of 1972–1973 and a corrected version of it that takes proper account of $\varepsilon_{D\infty}$, the corrected modulus formalism (CMF), demonstrates that the role played by $\varepsilon_{D\infty}$ (or ε_∞) in the OMF is incorrect. Detailed fitting of data for three different ionic glasses using a Kohlrausch–Williams–Watts response model, the KWW_1, for OMF and CMF analysis clearly demonstrates that the OMF leads to inconsistent shape-parameter (β_1) estimates and the CMF does not. The CMF KWW_1 model is shown to subsume, correct, and generalize the recent disparate scaling/fitting approaches of Sidebottom, León, Roling, and Ngai. © *2001 American Institute of Physics.*
[DOI: 10.1063/1.1374480]

I. INTRODUCTION AND BACKGROUND

Scaling is a method of treating data that allows one to subsume a mass of small-signal frequency-response data by means of a master curve whose shape is independent of an independent variable, such as temperature or mobile-ion concentration. The well-known time–temperature superposition approach is an example of scaling. In the immittance spectroscopy field, two almost orthogonally disparate types of scaling have been advocated and illustrated by different groups. It is always exciting when such different points of view are proposed because it raises the possibility that perhaps the two seemingly different approaches deal with different aspects of an only dimly seen larger whole, as in the parable of the blind men and the elephant. The present work is an effort to bring the two viewpoints closer together, and thus to delineate the underlying response structure: trunk, tail, and all, in a more complete fashion.

There are four related complex levels at which a given set of data may be presented: the complex dielectric constant level, $\varepsilon(\omega) = \varepsilon'(\omega) - i\varepsilon''(\omega)$; the complex conductivity level, $\sigma(\omega) = [i\omega\varepsilon_V\varepsilon(\omega)] = \sigma'(\omega) + i\sigma''(\omega)$; the complex resistivity level, $\rho(\omega) = 1/\sigma(\omega) = \rho'(\omega) + i\rho''(\omega)$; and the complex electric modulus level, $M(\omega) = i\omega\varepsilon_V\rho(\omega) = M'(\omega) + iM''(\omega) = 1/\varepsilon(\omega)$. Here, ε_V is the permittivity of vacuum and $\omega = 2\pi\nu$ is the radial frequency.

One group (e.g., Refs. 1–9; see further early references in Ref. 8) has proposed that scaling of $\sigma'(\omega)$ data is most appropriate, and when scaling is applicable it should involve the general form

$$\sigma'(\omega)/\sigma_0 = F(\omega\tau_S), \qquad (1)$$

where $\sigma_0 \equiv \sigma(0) \equiv 1/\rho_0$; F is a function describing the master scaling curve; and τ_S is a scaling relaxation time whose choice is the crucial element of the scaling, as discussed below. For experimental data, plots of $\sigma'(\omega)/\sigma_0$ vs. $\omega\tau_S$ for different values of an independent variable should lead to a single curve if scaling applies and if the values of the σ_0 and τ_S scaling parameters for each data set are appropriately chosen, not necessarily a straightforward task. On the other hand, when the form of F is known it can be used to generate synthetic data for specified values of its parameters. Then, scaling will apply as long as any shape parameters of the model are independent of an independent variable such as temperature.

The second group has been concerned with scaling of $M''(\omega)$ data[10–18] by plotting $M''(\omega)/M''_{max}$ vs ω/ω_{Mp}, where M''_{max} is the value of $M''(\omega)$ at its peak, occurring at $\omega = \omega_{Mp} \equiv 1/\tau_{Mp}$. Incidentally, even when scaling of both $\sigma'(\omega)$ and $M''(\omega)$ proves possible, the value of τ_{Mp} is unequal to that of τ_S except for Debye response. The relaxation time τ_{Mp} has sometimes been identified as the most probable conductivity relaxation time,[12] but one should remember that

[a]Electronic mail: macd@email.unc.edu

there are peaks of $\rho''(\omega)$ and of the dielectric-loss curve as well, all generally unequal.

There is one crucial difference between scaling and/or analyzing $\sigma'(\omega)$ or $M''(\omega)$ data. This is because of all the eight possible real and imaginary immittance parts of the response, only $\sigma'(\omega)$ and $\varepsilon''(\omega)$ do not directly involve the important quantity $\varepsilon_\infty \equiv \varepsilon'(\infty)$, always $\geqslant 1$. This essential response element is discussed in detail in the next section. As pointed out by Dyre[19] in 1988 and discussed further by the present author,[20–23] a disadvantage of analyzing data at the electric modulus level (not to be confused with the electric modulus formalism discussed below) is that it compounds the effect of ε_∞ with that of $M''(\omega)$. Here, and hereafter, $M''(\omega)$ and similar quantities are taken to be associated with a response model, and so the experimental quantities $M''_{\mathrm{dat}}(\omega)$ and $M''(\omega)$ are necessarily different.

Although $M''_{\mathrm{dat}}(\omega)$ is still widely used for the scaling and analysis of data,[10–18,24] its appropriateness has recently been called in question[4,9,25,26] again. Nevertheless, we show herein how both $M''_{\mathrm{dat}}(\omega)$ and $\sigma'_{\mathrm{dat}}(\omega)$ may be used to obtain consistent data analysis and scaling by taking proper account of ε_∞. To do so, however, and to produce synthetic data for comparison with, or fitting to, experimental results requires an appropriate conductive-system fitting model for thermally activated relaxation response. We shall be dealing with two types of conductive-system dispersive (CSD_k) response, ones that will be distinguished by means of a subscript k, equal to 0 or 1. The Davidson–Cole small-signal frequency-response model is a possible choice,[27] but we shall instead follow the original electric modulus-formalism (OMF) approach[28–30] by starting with a $k=0$ CSD_0 stretched-exponential temporal response function,

$$\Phi(t) = \exp[-(t/\tau_o)^{\beta_0}]. \tag{2}$$

Here, τ_o is a characteristic relaxation time of the response and β_0 is a shape or stretching parameter associated with Kohlrausch–Williams–Watts (KWW_k) response for the $k=0$ choice.[31,32]

Unfortunately, no closed-form analytic expression for the conductive-system frequency response associated with the stretched exponential, here denoted as the KWW_0 model,[22,23,25] is available for arbitrary β_0. Although Fourier transformation of Eq. (2) has been used to obtain the CSD_k response, such an approach is inconvenient for direct complex-nonlinear-least-squares (CNLS) fitting of wide-range experimental data. Luckily, the free LEVM computer program[33] contains highly accurate subroutines for calculating the KWW_k response and for CNLS fitting with it.

A main feature of the macroscopic OMF approach is its transformation of a $k=0$ response function, such as the KWW_0, to another one that involves a related, but different, distribution of relaxation times function. Such transformation changes a CSD_0 model to a CSD_1 one. In the present situation, the frequency-response model derived from the KWW_0 model is termed the KWW_1, and although it involves a new $\beta = \beta_1$ shape parameter, it does not lead to stretched-exponential behavior.[25,26] This model is the main one considered herein, both because it is used in the OMF and in the corrected version of the OMF, the corrected-modulus formal-

ism (CMF), and because it has been found to be a good choice for fitting a variety of experimental data.

II. ε_∞, MODELS, AND SCALING

A. Some general relations and definitions

Because the nature, definition, and use of ε_∞ is crucial to the difference between the 1972–1973 OMF, which has been widely employed to date for data analysis since its publication, and the CMF corrected version of it, first proposed in 1996 and discussed thereafter,[22,23,25,26] it is important to consider the role of ε_∞ in some detail. Consider, first, a nonconducting dielectric material. In the absence of dielectric dispersion up to frequencies well beyond those common to immittance spectroscopy, the bulk dielectric constant arising from nonionic dipolar and electronic polarization is frequency independent in the experimental region; call it $\varepsilon_{D\infty}$.[22,23,34]

Hopping theories and Monte Carlo simulation of conductive systems generally do not include $\varepsilon_{D\infty}$, yet they involve a nonzero dielectric response, $\varepsilon_C(\omega)$, which exhibits dispersion. Further, both the OMF and the CMF generally use the specific KWW_1 model and lead to a $\varepsilon'_{C1}(\omega)$ response, with variation from $\varepsilon'_{C1}(0) \equiv \varepsilon_{C10}$ to $\varepsilon'_{C1}(\infty) \equiv \varepsilon_{C1\infty}$. Similarly, the KWW_0 model yields $\varepsilon_{C0}(0) \equiv \varepsilon_{C00}$ and $\varepsilon_{C0}(\infty) \equiv \varepsilon_{C0\infty}$. An important difference is, however, that for ordinary situations $\varepsilon_{C0\infty}$ is identically zero, and $\varepsilon_{C1\infty}$ is not zero within the usual experimental frequency range.[22,23,25]

Because $\varepsilon_{C1\infty}$ arises entirely from the presence of charge carriers such as ions in the material, at sufficiently high frequencies it will necessarily approach zero because of charge-carrier inertial effects. It seems likely that this final decrease towards zero of $\varepsilon_{C1\infty}$ will occur at somewhat lower frequencies than the relaxation of $\varepsilon_{D\infty}$ towards the square of the index of refraction. For the frequency range where $\varepsilon'_{C1}(\omega)$ is well approximated by a nonzero, frequency-independent $\varepsilon_{C1\infty}$, it may be considered to arise from dipolar-like motion of each charge carrier in a localized potential-well region without long-range hopping. If, indeed, the KWW_1 fitting model is more appropriate than the KWW_0 one, as suggested by considerable CMF data fitting results, then the above plausible physical explanation for nonzero $\varepsilon_{C\infty}$ requires that the KWW_1 be chosen rather than KWW_0. They both cannot apply in the region where $\varepsilon_{C\infty}$ is constant.

For a real conducting-system material, one expects that there must be dielectric contributions from both the underlying bulk material, $\varepsilon_{D\infty}$, and from mobile-charge effects, $\varepsilon_C(\omega)$, with these quantities independent of each other to first order. Then, omitting k subscripts, $\varepsilon_0 = \varepsilon_{C0} + \varepsilon_{D\infty}$ and $\varepsilon_\infty = \varepsilon_{C\infty} + \varepsilon_{D\infty}$. It follows that $\Delta\varepsilon_{\mathrm{dat}} = \varepsilon_{0\mathrm{dat}} - \varepsilon_{\infty\mathrm{dat}}$, which should be compared to $\Delta\varepsilon_0 = \varepsilon_{C00}$ or to $\Delta\varepsilon_1 = \varepsilon_{C10} - \varepsilon_{C1\infty}$, depending on whether one is fitting with a CSD_0 or CSD_1 model.

B. Some specific-model relations

The crucial difference between the OMF and the CMF is that the former sets $\varepsilon'_{C1}(\infty)$ identically equal to $\varepsilon_s \equiv \varepsilon_{D\infty}$ in its original version and to ε_∞ in later work, while for the

CMF $\varepsilon'_{C1}(\infty)=\varepsilon_{C1\infty}$. Further, proponents of the OMF generally do not identify ε_∞ as containing both contributions, and they implicitly seem to treat it as if it were $\varepsilon_{D\infty}$. Since the OMF is thus taken to account for $\varepsilon_{D\infty}$ effects directly, no separate free $\varepsilon_{D\infty}$ parameter is used in OMF fitting to data. But, in both the CMF and the KWW$_0$, such a parameter is necessarily included in fitting. It follows that OMF fits yield an estimate of $\varepsilon_\infty=\varepsilon_{C1\infty}+\varepsilon_{D\infty}$ but deal with it as if it were $\varepsilon_{D\infty}$. In contrast, CMF fits yield separate estimates of $\varepsilon_{D\infty}$ and $\varepsilon_{C1\infty}$, and as shown previously[22,23,25] and in Sec. IV, such fits of experimental data are both much better than OMF fits and, unlike them, yield consistent parameter estimates.

It is unnecessary to discuss additional physical reasons why the CMF should replace the OMF since this matter has already been considered in detail,[22,23,26,35] but in any event, the choice between them should ultimately depend upon their fitting performance, as particularly illustrated in Sec. IV. It is, however, worth mentioning that the general form of macroscopic CSD$_1$ CMF response agrees exactly with that of a continuous-time-random-walk microscopic hopping model,[36] while the OMF response does not.[26,35] Such agreement with a microscopic theory that does not involve long-range Coulomb interactions illuminates the physics underlying the CMF response and, in view of the excellent fitting ability of the KWW$_1$ CMF model, widens the range of appropriateness of both the microscopic and macroscopic treatments.

We next summarize some important limiting-frequency relations that are intrinsic properties of dispersive relaxation response,[22,23,25,26] when, as usual, it can be represented, at least mathematically, by a normalizable distribution of relaxation times (DRT). Each relation shows, first, the general CSD$_k$ form and then the specific result for the KWW$_0$ or CMF KWW$_1$ model. The general forms involve moments of the DRT,[22,23] such as $\langle\tau\rangle\equiv\tau_o\langle x\rangle$, where $x\equiv\tau/\tau_o$ and $\langle x\rangle$ depends only on the shape of the distribution. In order to distinguish between the appropriate relations for τ_o, the characteristic relaxation time of the distribution for the various cases, we employ the notation $(\tau_o)_{k\omega}$, where $k=0$ or 1 and $\omega=0$ or ∞. Then using the relations $\langle x^{-1}\rangle_1=\langle x\rangle_{01}^{-1}$ and $\langle x\rangle_1=\langle x^2\rangle_{01}/\langle x\rangle_{01}$,[22,23] one obtains

$$(\tau_o)_{00}/\varepsilon_V=\varepsilon_{C00}\rho_0/\langle x\rangle_0=\Delta\varepsilon_0\rho_0/\langle x\rangle_0$$
$$=\Delta\varepsilon_0\rho_0\beta_0/\Gamma(1/\beta_0), \qquad (3)$$

$$(\tau_o)_{0\infty}/\varepsilon_V=\varepsilon_{C0\infty}\rho_0\langle x^{-1}\rangle_0, \qquad (4)$$

$$(\tau_o)_{10}/\varepsilon_V=\varepsilon_{C10}\rho_0/\langle x\rangle_1$$
$$=\varepsilon_{C10}\rho_0\langle x\rangle_{01}/\langle x^2\rangle_{01}$$
$$=\varepsilon_{C10}\rho_0\Gamma(1/\beta_1)/\Gamma(2/\beta_1), \qquad (5)$$

$$(\tau_o)_{1\infty}/\varepsilon_V=\varepsilon_{C1\infty}\rho_0\langle x^{-1}\rangle_1$$
$$=\varepsilon_{C1\infty}\rho_0/\langle x\rangle_{01}=\varepsilon_{C1\infty}\rho_0\beta_1/\Gamma(1/\beta_1). \qquad (6)$$

In the above equations, $\Gamma(\ )$ is the Euler gamma function,[37] and Eq. (4) is only included for completeness since $\langle x^{-1}\rangle_0=\infty$ and so $\varepsilon_{C0\infty}=0$, except when the distribution is cut off in the small-τ region.[22] The 01 subscripts

indicate that the relevant CSD$_0$ distribution involves a $k=1$ shape parameter, such as β_1, as shown for the right-most parts of the $k=1$ equations. Because Eqs. (5) and (6) involve the same model, $(\tau_o)_{10}=(\tau_o)_{1\infty}=\tau_o$. The above results show that $\varepsilon_{C1\infty}=\varepsilon_{C00}=\Delta\varepsilon_0$ only when $(\tau_o)_{00}=(\tau_o)_{1\infty}$, requiring conditions not found from experimental data fits. It is noteworthy that if β_1 varies from 0.3 to 0.7, perhaps because of temperature changes, then the factor $\beta_1/\Gamma(1/\beta_1)$ in Eq. (6) varies from about 0.11 to 0.79 and reaches unity for $\beta_1=1$.

For CSD$_1$ KWW$_1$ situations, it follows from Eqs. (5) and (6) that

$$\Delta\varepsilon_1=(\tau_o/\varepsilon_V\rho_0)[\langle x\rangle_1-\langle x^{-1}\rangle_1^{-1}]=\varepsilon_{C1\infty}f(\beta_1), \qquad (7)$$

where

$$f(\beta_1)\equiv[(\langle x^2\rangle_{01}/\langle x\rangle_{01}^2)-1]=[\{\beta_1\Gamma(2/\beta_1)/\Gamma(1/\beta_1)^2\}-1]. \qquad (8)$$

Note that $f(0.3)/f(0.7)\cong26.4$. Let us now introduce a standard expression for σ_0, namely,

$$\sigma_0=[\gamma N(qd)^2/6kT]/\tau_H, \qquad (9)$$

where γ is the fraction of charge carriers of charge q that are mobile, N is the maximum mobile-charge number density, d is the rms single-hop distance for a hopping entity, and τ_H is a hopping time. It has been shown[26,35,36] that for CSD$_1$ behavior $\tau_H=\langle\tau\rangle_{01}$, leading to the following important result:

$$\varepsilon_{C1\infty}=\sigma_0\langle\tau\rangle_{01}/\varepsilon_V=\sigma_0\Gamma(1/\beta_1)/\beta_1\varepsilon_V$$
$$=[\gamma N(qd)^2/6kT\varepsilon_V]. \qquad (10)$$

For CSD$_0$ situations, on setting $\tau_H=\langle\tau\rangle_0=\tau_o\Gamma(1/\beta_0)/\beta_0$, one obtains, if $\rho_{01}=\rho_{00}$,

$$\varepsilon_{C00}=\Delta\varepsilon_0=[\langle\tau\rangle_0/\langle\tau\rangle_{01}]\varepsilon_{C1\infty}=\langle\tau\rangle_0\sigma_0/\varepsilon_V. \qquad (11)$$

For the CMF, the tau ratio in Eq. (11) is about 0.45 when $\beta_1=0.4$ and $\beta_0=1-\beta_1$. Sidebottom[6] has presented a result for $\Delta\varepsilon_0$ derived by an approximate approach that is similar to that of the right-most part of Eq. (10) except that the factor of 6 in Eq. (10) is replaced by 3 and he does not include an equation for $\Delta\varepsilon_0$ comparable to Eq. (11).

C. Approximate and exact-scaling relations

Interest in scaling has been recently renewed by the work of Roling et al.,[1] Sidebottom,[6] Sidebottom, Roling, and Funke,[9] Schrøder and Dyre,[38] and Dyre and Schrøder.[8] Some early history of scaling is discussed in Ref. 8. A virtue of the scaling approach is that it may be applied directly to the relevant data and no model fitting is required in the ideal case. But, as Eq. (1) indicates, $\sigma'(\omega)$ scaling requires estimates of σ_0 and τ_S values. For most conductive-system experimental results, non-negligible electrode effects and noise appear in low-frequency $\sigma'(\omega)$ and $\varepsilon'(\omega)$ data and may be large enough to reduce the accuracy of σ_0 and ε_0 estimates obtained directly from the data. Reliable estimation of ε_0, a quantity often needed in calculating τ_S, is especially difficult without model fitting when there is little or no evidence of a plateau in $\varepsilon'(\omega)$ as the frequency is decreased, as is often the case. Finally, scaling requires that shape parameters such

as β_k be temperature independent over the range of interest. In contrast, fitting of composite models that include both bulk and electrode response functions, as in Sec. IV below and in Refs. 22, 23, 25, 26, often allows one to obtain good estimates of all parameters, including possibly temperature-dependent shape ones. If the shape parameters are found to remain constant, then one obtains a temperature-independent master fitting model in lieu of a master response curve.

If one believes that a CSD_0 model is appropriate for the data, it is only necessary to set τ_S equal to the $(\tau_o)_{00}$ of Eq. (3). As mentioned in the preceding section, Sidebottom[6] independently proposed a semiempirical version of this result, one without the factor $\langle x \rangle_0$ and with $\Delta\varepsilon_0$ taken as twice the $\varepsilon_{C1\infty}$ of Eq. (10). For scaling of response involving temperature-independent shape parameters, $\langle x \rangle_0$ will remain constant, so its absence in Sidebottom's approach is of no consequence. But, it is an important part of the expression for τ_S when shape varies and model fitting is carried out.

For the CMF KWW$_1$ situation, one can set the quantity $(\tau_o)_{10} = (\tau_o)_{1\infty} = \tau_o$ equal to τ_S, thus involving either ε_{C10} or $\varepsilon_{C1\infty}$. Again, if time-temperature superposition applies, the dimensionless moments of the DRT present in Eqs. (5) and (6) will be constant and may be ignored for scaling. Further, we can, under such conditions, set $\tau_S = \varepsilon_V \Delta\varepsilon_1 / \sigma_0$, similar to the Sidebottom result when $\Delta\varepsilon_1$ is given by Eq. (7), with $f(\beta_1)$ ignored or taken constant, and with $\Delta\varepsilon_1$ set equal to $\Delta\varepsilon_{dat} = \varepsilon_{0dat} - \varepsilon_{\infty dat}$. We, thus, see that for scaling the Sidebottom approach is appropriate whether the underlying data are best represented by a CSD_0 model or a CSD_1 one. But, when one wishes to use Eq. (10) to estimate values of the rms hopping distance d,[6,26,39] one must recognize that $\Delta\varepsilon_0$, $\Delta\varepsilon_1$, and $\varepsilon_{C1\infty}$ are different quantities and, therefore, either Eq. (7) or (11) must be employed. Of course, CMF fitting leads to an estimate of $\varepsilon_{C1\infty}$ that can be directly used with Eq. (10).

Ngai and Rendell[40] and León, Lunkenheimer, and Ngai[41] have used an OMF model for data analysis and scaling which involves an equation equivalent to Eq. (7) except with $\varepsilon_{C1\infty}$ replaced by $\varepsilon_{D\infty}$, but called ε_∞. Thus, such an approach equates $\varepsilon_{\infty dat}$ with $\varepsilon_{D\infty}$, taken essentially temperature independent as well as independent of mobile-charge concentration, instead of with $\varepsilon_\infty = \varepsilon_{C1\infty} + \varepsilon_{D\infty}$, which can depend on both. The present CMF approach involves $f(\beta_1)$, $\varepsilon_{C1\infty}$, and $\varepsilon_{D\infty}$ dependence. Thus, it combines the Sidebottom approach,[6] which involves only $\Delta\varepsilon \propto \varepsilon_{C1\infty}$ dependence, with that of $f(\beta_1)$, as in the OMF Ngai–León work, together with a separate account of $\varepsilon_{D\infty}$ as required by the CMF. Unlike the Sidebottom result, which involves only N but no shape dependence, and the Ngai–León analysis, which involves shape dependence but no mobile-charge dependence through N, the present results[26,35] involve both dependencies. As shown in Ref. 26 and below in Sec. IV, the CMF approach thus leads to better and more consistent fits and parameter estimates than does the OMF.

III. $M''(\omega)$ SCALING SIMULATIONS

Here, we illustrate scaling behavior for the KWW$_1$ and KWW$_0$ response models discussed above. Figure 1 shows
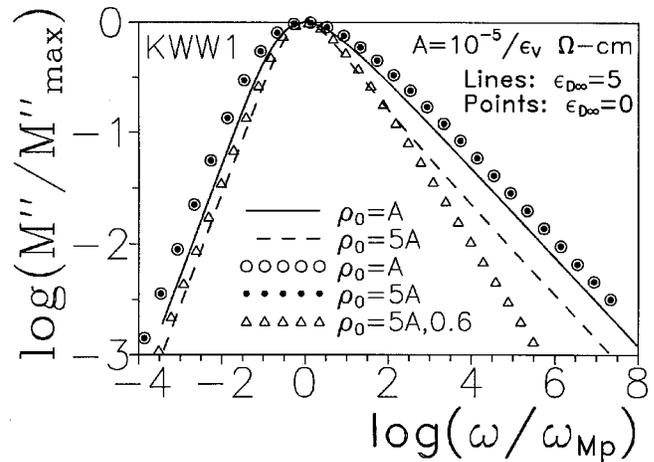

FIG. 1. Scaling attempts using synthetic KWW$_1$ bulk $M''(\omega)$ data, with and without the separate inclusion of $\varepsilon_{D\infty}$ effects. The value of the shape parameter β_1 is 0.4 for all results except that defined by open-triangle symbols where it is 0.6. For all the results, the characteristic relaxation time τ_o was set to 1.5×10^{-5} s, and ω_{Mp} is defined as the angular frequency at the M''_{max} peak of the $M''(\omega)$ curve. Here, and subsequently, $A = 10^{-5}/\varepsilon_V$ Ω cm.

such results for the KWW$_1$ model with $\beta_1 = 0.4$ for the top four situations listed in the legend and 0.6 for the bottom one. The τ_o parameter value was held constant at 1.5×10^{-5} s, and only the ρ_0 value was varied in calculating the present virtually exact responses. Those results depicted with lines involve the usual CMF situation in which a separate $\varepsilon_{D\infty}$ parameter is included in the total response model in addition to $\varepsilon_{C1\infty}$, which arises entirely from mobile charges. The three responses shown by points alone were calculated without the inclusion of $\varepsilon_{D\infty}$, and so they represent pure bulk KWW$_1$ conductive-system behavior.

Comparison of the solid and dashed lines indicates that no scaling is possible when ρ_0 alone is varied. Note that although the $\beta_1 = 0.6$ response designated by open-triangular points is quite similar to the comparable $\beta_1 = 0.4$ dashed line over the range from the peak value of the ordinate down to about a value of 0.1, it properly approaches its limiting high-frequency log–log slope of $-\beta_1 = -0.6$, quite different from the limiting -0.4 slope of the dashed line. But, the similarity between the dash-line result and that involving open-triangle symbols in the region down to about 0.1 of the peak of M'' implies that those OMF methods which rely on obtaining an estimate of β_1 from the width of an experimental response curve at half height[28–30,42] are unlikely to lead to adequate estimates.[22,26] This is because they compare an experimental curve that always includes $\varepsilon_{D\infty}$ effects with OMF-model results that do not properly include such effects, just the situation illustrated here.

Since the solid and open-circle responses shown in Fig. 1 agree perfectly, it is clear that exact M'' scaling occurs when either synthetic data, as here, involves no $\varepsilon_{D\infty}$ contribution or when an accurate estimate of $\varepsilon_{D\infty}$ is subtracted from experimental data, usually requiring a CNLS fit of the original data in order to obtain such an estimate and then using a program like LEVM to subtract its effects. Because such manipulation of experimental results is unfortunately rare, if such data were better fitted by the CMF rather than by
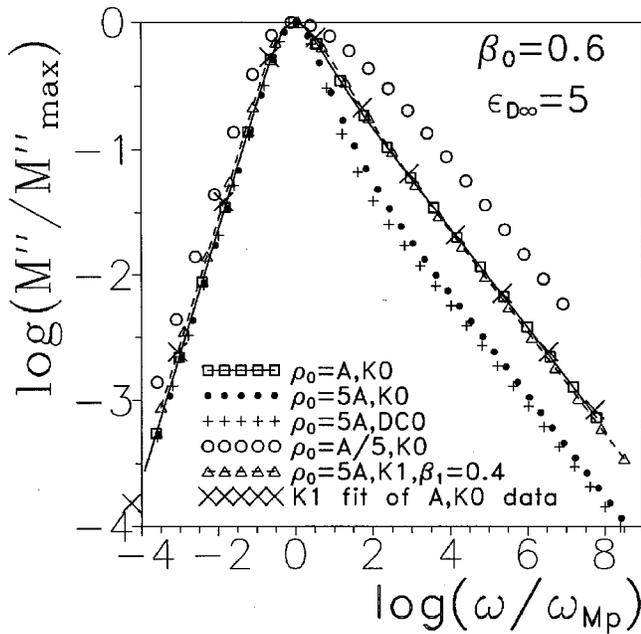
FIG. 2. Scaling attempts using synthetic KWW$_0$ (designated K0) bulk $M''(\omega)$ data with $\beta_0 = 0.6$ and KWW$_1$ (designated K1) data with $\beta_1 = 0.4$ for the curve with open-triangular symbols and 0.384 for the fitted one with X X symbols. In addition, a curve for a Davidson–Cole response model with its exponent equal to 0.6 is included and designated as DC0.

the OMF (see comparative examples below), scaling of the unmodified data would fail in those situations where τ_o and ρ_0 do not vary proportionately and/or where β_1 does not remain constant. Such proportionate behavior is closely found for temperature variation for usual thermally activated response, but not for isothermal data for the same material but with different mobile-ion concentrations.

Note that even when τ_o and ρ_0 involve the same activation energy, they will only vary proportionately under temperature variation for the KWW$_1$ response provided that $\varepsilon_{C1\infty}/\langle x \rangle_{01}$ is temperature independent, as shown by Eq. (6). Thus, when β_1 is temperature independent, necessary for scaling to work, $\varepsilon_{C1\infty}$ must also be. There is some evidence, however, that $\varepsilon_{C1\infty}$ may vary as $1/T$,[23,43] resulting in $T\sigma_0$ being proportional to $1/\tau_o$, rather than τ_o and ρ_0 being fully proportional. For usual activation energy magnitudes, thermally activated exponential variation with T dominates that of a preexponential T factor itself, so when this failure of exact proportionality occurs, scaling may still appear adequate for data with ordinary-size experimental errors and for limited temperature variation.

Figure 2 is similar to Fig. 1 but primarily involves the KWW$_0$ response with $\beta_0 = 0.6$ and τ_o again fixed. If $\varepsilon_{D\infty}$ were subtracted from these KWW$_0$ results, there would no longer be a peak in $M''(\omega)$ since $\varepsilon_{C0\infty} = 0$, so $M''(\omega)$ would increase indefinitely with increasing frequency. Comparison of the three KWW$_0$ lines shows again that scaling does not work when τ_o and ρ_0 variation is not proportional, so even when β_0 is temperature independent attempted scaling of data with different ionic concentrations will fail. The CSD$_0$ Davidson–Cole-model DC0 response is included here to show that it yields very similar results to those of the KWW$_0$

model with the same ρ_0 choice and an exponent value of 0.6.

Figure 2 also includes two different KWW$_1$ responses. The line with triangular points lies close to the KWW$_0$ line with open-square points, and its limiting high-frequency slope, $\beta_1 - 1 = -\beta_0 = -0.6$, is necessarily the same as those of the KWW$_0$ responses shown. Although it is thus not surprising that the final slopes are the same, it is remarkable that the open-square and open-triangular point lines agree so well over the full-frequency range shown. Although they involve the same $\tau_o = 1.5 \times 10^{-5}$ s value, their dc resistivities differ by a factor of 5.

The second KWW$_1$ response is shown for clarity with only a few points, the X X symbols, and it also agrees well with the open-square KWW$_0$ line. These results were obtained by fitting the original $M''(\omega)$ data with the KWW$_0$-and-$\varepsilon_{D\infty}$ model with all fit parameters free to vary. The result led to a value of the relative standard deviation of fit, S_F, of about 0.0372, a fairly poor fit value, and to the following parameter estimates: $\varepsilon_{D\infty} = 4.34$, $\tau_o = 2.05 \times 10^{-6}$s, $\rho_0 = 1.013A$, and $\beta_1 = 0.384$. We see that although the dc resistivity is close to that of the KWW$_0$ data, the τ_o estimate is much smaller and the β_1 one is only slightly smaller than 0.4. It is quite surprising that two KWW$_1$ data sets with some quite different parameters can be scaled to yield nearly the same scaled response on a log–log plot. Incidentally, fitting of the $5A$,K1 exact KWW$_1$-and-$\varepsilon_{D\infty}$ data set to the KWW$_0$ model led to $S_F \simeq 0.032$ and $\beta_0 \simeq 0.587$.

In summary, the present results indicate that no modulus scaling is possible unless the shape parameter, here β, is temperature independent and both τ_o and ρ_0 vary proportionately with temperature or mobile-ion concentration. Although Ghosh and Sural[7] have shown that their $\sigma'(\omega)$ fluoride–glass data can be scaled for both temperature and composition variation, the same data expressed at the modulus level cannot be scaled by the present approach for different charge-carrier concentrations, in accordance with present predictions.

IV. ORIGINAL AND CORRECTED ELECTRIC-MODULUS-FORMALISM DATA-FITTING RESULTS

The OMF continues to be almost exclusively used for modulus-formalism (MF) fitting of data on conducting glasses (e.g., see Refs. 20 and 44, and references therein), in spite of publications since 1996 pointing out its defects and discussing a corrected version,[22,23,25,26,35,45] the CMF. Therefore, further reasons to retire the OMF in favor of the CMF are evidently needed. Since appropriateness in fitting experimental data is an ultimate and necessary requirement for acceptance of a theory, fitting comparisons between the two models, not previously carried out in detail for experimental data, are clearly desirable. The present comparisons use weighted complex-nonlinear-least-squares fitting of the accurate KWW$_1$ model and involve direct LEVM estimation of β_1 for situations where $\varepsilon_{D\infty}$ may influence the result and those where it does not.

The results in Fig. 3 were obtained on fitting $M''(\omega)$ and $\sigma'(\omega)$ data for the LAS–glass, Li$_2$O·Al$_2$O$_3$·2SiO$_2$, first

FIG. 3. OMF and CMF KWW_1 fits of $M''(\omega)$ $Li_2O \cdot Al_2O_3 \cdot 2SiO_2$ data and their β_1 estimates for comparison with the β_1 estimate from a fit of the $\sigma'(\omega)$ response of the same data. Here, and elsewhere, $\nu_n = 1$ Hz.
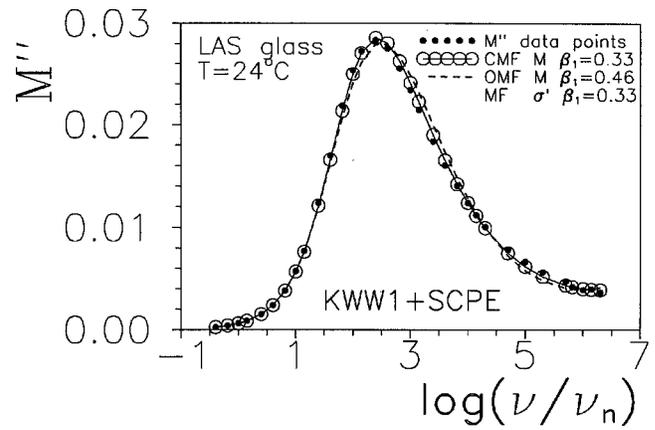
FIG. 4. Fits like those of Fig. 3 except that here the composite fitting model included both the KWW_1 response and that of a constant-phase element in series with it.

analyzed in the original 1972–1973 modulus-formalism publications[29,30] and later as well.[46] We see that although the CMF fits the data better than the OMF, neither one fits the higher-frequency points well. Thus, the actual S_F fit values are poor, being about 0.15, 0.24, and 0.12 for the CMF, OMF, and MF fits, respectively. Further, and most important, the CMF β_1 estimate, which involves fitting $M''(\omega)$ data with the KWW_1 model and a separate free $\varepsilon_{D\infty}$ parameter, agrees with that obtained from a fit of the $\sigma'(\omega)$ data, one where the presence or absence of $\varepsilon_{D\infty}$ is entirely immaterial since it appears only in $\sigma''(\omega)$. Thus, the CMF and MF fits yield consistent estimates while the OMF and MF ones do not. Incidentally, the earlier OMF fits led to a β_1 estimate of 0.47,[30,46] but the fit procedure used was much less accurate than that instantiated in LEVM. Further, the present fits use all the original 33 data points while earlier ones used only a subset of 27 of those points.

The OMF analyses of the present data are inconsistent in another way as well, one different from the differences in identification and meaning of $\varepsilon'_{C1}(\infty)$ between the OMF and CMF approaches already discussed. Earlier OMF estimates of $\langle \tau \rangle$ values were about 4.5×10^{-4} s (Ref. 30) and 8.2×10^{-4} s.[46] But, ignoring their numerical difference, they both set $\langle \tau \rangle = \langle \tau \rangle_0$, amounting to the use of a KWW_0 expression for a KWW_1 OMF situation. The actual mean relaxation time for the latter and present situation is $\langle \tau \rangle_1 = \langle \tau^2 \rangle_{01} / \langle \tau \rangle_{01}$,[22,23] which can be expressed for the KWW_1 model as $\tau_o \Gamma(2/\beta_1)/\Gamma(1/\beta_1)$, quite different from the pure $\langle \tau \rangle_0$ formula. For the $\beta_1 \simeq 0.44$ OMF fit of Fig. 3, carried out with unity weighting to emphasize the upper part of the $M''(\omega)$ response, the τ_o estimate was close to that cited in Ref. 46, but $\langle \tau \rangle_1$ was about 4.4×10^{-3} s.

Figure 4 involves fitting the data of Fig. 3 with the KWW_1 conductive-system-response model as before, but with a constant-phase element (CPE) added in series at the complex resistivity level. This element, here designated by SCPE, is included to account for electrode effects and may be expressed as $\rho_{SC}(\omega) = 1/[\varepsilon_V A_{SC}(i\omega)^{\gamma_{SC}}]$, where $0 < \gamma_{SC} \leq 1$ and the constant A_{SC} is an ordinary dielectric constant when $\gamma_{SC} = 1$.[47] Its addition leads to very much improved

fits, with S_F values of 0.027, 0.05, and 0.028, but the OMF fit is obviously still much poorer than the others.

As before, the present results show that the CMF and MF fits are consistent while the OMF and MF ones are not. Although the β_1 and $\langle \tau \rangle_1$ estimates differ from those of Fig. 3, the Fig. 4 fits much better represent the bulk KWW_1 response. Incidentally, the CMF fit here yielded an estimate of $\langle \tau \rangle_1 \simeq 2.7 \times 10^{-3}$ s for the CMF bulk response alone, quite different from the Moynihan OMF values cited above. Since comparison of the results shown in Figs. 3 and 4 indicates that the effects of the SCPE are significant here only at high frequencies, it is of interest to compare the results of KWW_1 CMF and OMF fits of the original data after the deletion of the seven highest-frequency points and with the SCPE term not included in the fitting model. One then obtains β_1 estimates of 0.33 and 0.454, consistent with the composite-model fits as expected, although the KWW_1+SCPE fits are more appropriate and better.

Incidentally, the value of the high-frequency-limiting power-law exponent associated with the Fig. 4 CMF KWW_1 response, $(1 - \beta_1)$, is about 0.67 while the γ_{SC} estimate here was about 0.64. Figure 5 presents log–log curves of the real and imaginary parts of the CMF $M(\omega)$ and $\sigma(\omega)$ fit results compared to the actual data points (solid circles). Also shown are the associated β_1 estimates for individual real- and imaginary-part $\sigma(\omega)$ CMF and OMF fits. Again, the CMF results are consistent and the OMF ones are not.

Figure 6 shows fit results for a different glass, $Na_2O \cdot 3SiO_2$.[48] Here, better account of deviations from the pure KWW_1 response was accomplished by adding a ZC response element in series with the KWW_1 response.[25,47] Specific ZC response at the complex resistivity level may be expressed as $\rho_{ZC}(\omega) = \rho_{ZC0}/[1 + \rho_{ZC0} G(i\omega)^{\gamma_{ZC}}]$, a form which approaches the SCPE as ρ_{ZC0} becomes sufficiently large. For the present fits, since the ρ_0/ρ_{ZC0} ratio was about 3400, the ZC element only significantly affected the high-frequency part of the combined response, a region where it approximated CPE behavior. The estimated value of the ZC power-law exponent, γ_{ZC}, was about 0.74 for the CMF fits and 0.93 for the OMF one.
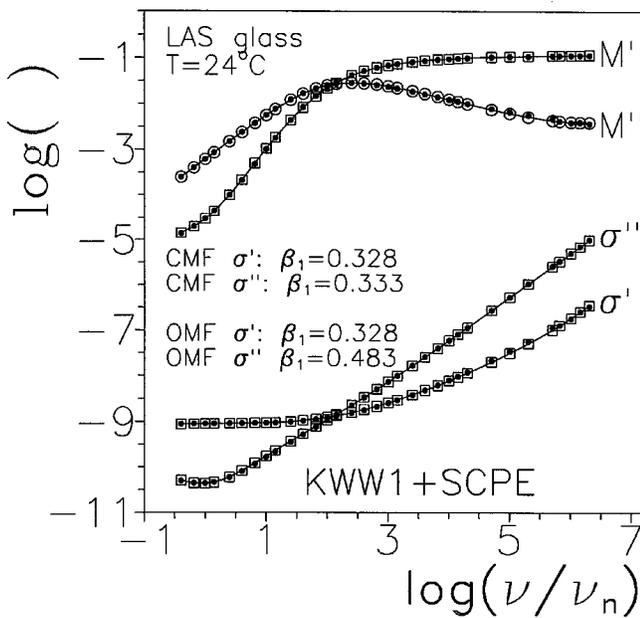
FIG. 5. Fit results (open symbols) and data (solid circles) for CNLS composite-model fitting of LAS–glass data as in Figs. 3 and 4.

The Fig. 6 data are appreciably more accurate than the LAS–glass ones, so the S_F values were found to be about 10 or 20 times smaller than those for Fig. 4, as shown in Fig. 6. Differences from earlier fits of these data[23,25] arise principally from the omission here of one outlying point. The CMF fit results for the composite model, open squares, are compared in the Fig. 6 with those for which the ZC-fit contribution to the data was subtracted from the original data and the resulting data fitted again with just the CMF KWW_1 model. Note that there is no significant difference between the open-square and open-circle points until $M''(\omega)$ has decreased to half height. Finally, the CMF β_1 estimates are again consistent and the OMF ones are not. Note that a complex CMF $\sigma(\omega)$ fit yielded a β_1 estimate of 0.4033, very close to the mean of the $\sigma'(\omega)$ and $\sigma''(\omega)$ individual fit estimates of 0.415 and 0.393, respectively.
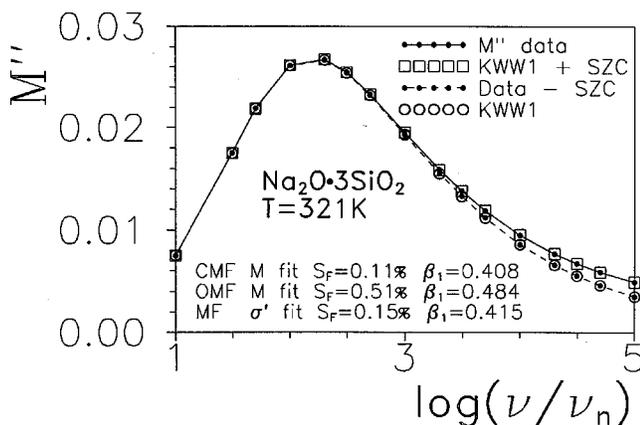

FIG. 6. Results of fitting $Na_2O \cdot 3SiO_2$ data with a composite model including a ZC element and without that element. Here, S_F is the relative standard deviation of a fit.

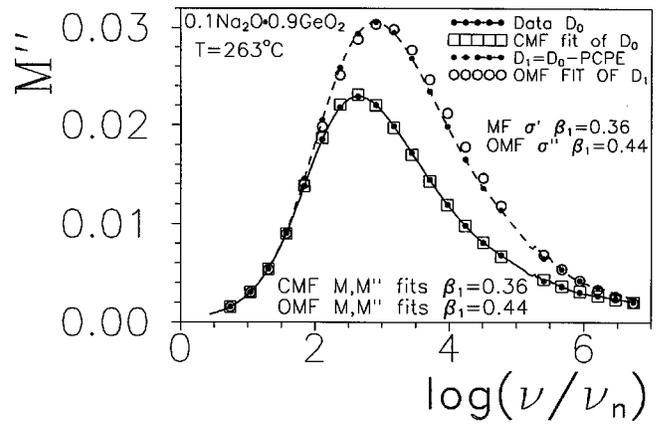FIG. 7. Results of fitting $0.1Na_2O \cdot 0.9GeO_2$ data with a composite model involving a KWW_1 response model and a constant-phase element in parallel electrically with it, and with the effects of that element subtracted from the data.

The last material to be considered is $x_c Na_2O \cdot (1-x_c) GeO_2$, with x_c, the mole fraction, equal to 0.1 for the Fig. 7 results. These data[6] are noisy, particularly in the low- and high-frequency regions, so fits of only the middle-region data are presented. The lower line shows the results of a CMF fit of that data using the KWW_1 model in *parallel* with a CPE, the PCPE. Although with good data LEVM allows one to distinguish between using a CPE or ZC in series with the bulk model or such an element in parallel, here both approaches yielded about the same fit quality and their results were nearly indistinguishable in a plot like that of Fig. 7.

Therefore, for variety the results of using the PCPE are illustrated here. This element may be expressed at the complex dielectric constant level as $\varepsilon_{PC}(\omega) = A_{PC}(i\omega)^{-\gamma_{PC}}$, where A_{PC} is a constant and $0 < \gamma_{PC} \leq 1$. This distributed element, therefore, leads to a high-frequency-limiting power-law exponent at the complex conductivity level of $(1 - \gamma_{PC})$. Since the estimated value of γ_{PC} was about 0.02 here, the associated log–log slope was about 0.98, an apparent instance of "nearly constant loss."[48–50] But, the alternate fit including a series rather than a parallel additional element led to $\gamma_{ZC} \approx 0.79$, clearly not an instance of nearly constant loss. Therefore, in cases like the present, one should be wary of asserting that nearly constant loss is an identifiable part of the overall response.

The top line in Fig. 7 shows an OMF fit of the data with the effect of the parallel CPE subtracted. Unlike the subtraction of a series element in the composite-fit models of Figs. 4–6, subtraction of an added parallel element results in a significant increase in the peak value of $M''(\omega)$, as shown here. Here again, the β_1 estimates presented in Fig. 7 are consistent for CMF fits and inconsistent for OMF ones. $M(\omega)$ fitting of the data after subtraction of the PCPE element, led to a CMF β_1 estimate of about 0.365 ± 0.002 and an OMF one of about 0.425 ± 0.001. The S_F value for the latter fit, 0.042, was, however, more than twice as large as that of the former one.

In summary, all the fits shown in Figs. 3–7 for three different glasses yield consistent CMF results and strongly inconsistent OMF ones. These data-fit comparisons un-
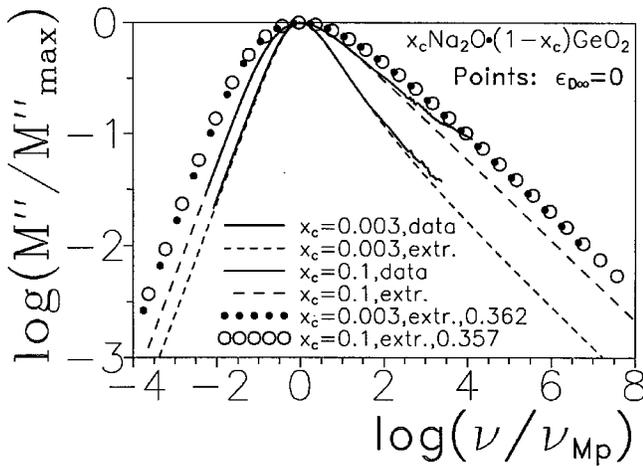
FIG. 8. $M''(\omega)$ scaling results for x_c Na$_2$O$\cdot$(1$-x_c$) GeO$_2$ data for two values of x_c. Here, ν_{Mp} is the frequency at the peak of the $M''(\omega)$ curve. Curves designated by ''extr.'' are extrapolated using model parameters estimated from the data fitting. The numbers listed for the results involving points are estimated β_1 values obtained from separately fitting these results, ones which involve data with the effects of $\varepsilon_{D\infty}$ subtracted.

FIG. 9. $\sigma'(\omega)$ scaling results for the same material as in Figs. 7 and 8 and for synthetic data sets. Here, τ_S, the scaling relaxation time, is set equal to appropriate τ_o fit estimates, such as that from the data fit whose results are shown in Fig. 7, or to $r\tau_o$, where τ_o is the value used in calculating synthetic data. For such data in this figure, $\rho_0=(10^{-5}/\varepsilon_V)B$ Ω cm and $\tau_o=1.5\times10^{-5}C$ s, where $r=1$ for the left-most synthetic curve and 5.43 for the right one.

equivocally indicate that the CMF is a proper and usually appropriate fitting model and that the OMF is always inconsistent. Therefore, it should no longer be used.

V. SOME SCALING RESULTS FOR EXPERIMENTAL DATA WITH DIFFERENT MOBILE-ION CONCENTRATIONS

Here, we illustrate two kinds of scaling for the x_c Na$_2$O(1$-x_c$) GeO$_2$ glass with $x_c=0.1$, as in Fig. 7, and also $x_c=0.003$. Figure 8 shows scaled $M''(\omega)$ results for the original data for these two concentrations, and, in addition, extrapolations of these data sets derived from the CMF KWW$_1$ parts of the fits of the data. It is clear that these data sets do not scale properly, just as one would expect from the discussion and illustrations of Sec. III. But, if one generates synthetic data from the fits which led to the extrapolated dashed lines but omits $\varepsilon_{D\infty}$ effects completely, one obtains the two sets of points shown. Since they lie on the same line, scaling works perfectly, showing that it is the presence of ubiquitous $\varepsilon_{D\infty}$ effects in such data sets that lead to their failure to scale properly.[22]

We turn now to scaling at the $\sigma'(\omega)$ level and show results for both the above data sets and synthetic ones. The two experimental-data lines in Fig. 9 used values of the σ_0 and τ_S scaling parameters derived from best CMF fits of the midrange data, as in the results of Fig. 7. Thus, one should not expect good scaling except for these portions of the data. Except for some evident irregularities, particularly in the lower-concentration data, we do indeed observe adequate scaling in these regions. Note that the τ_S values used here satisfy Eq. (6), and so involve $\varepsilon_{C1\infty}$ rather than the $\Delta\varepsilon=\tau_o\sigma_0/\varepsilon_V$ expression used by Sidebottom[6] and Dyre[8,38] for scaling of these same data sets. Their expression is adequate for scaling when a shape parameter such as β_1 is temperature independent, as discussed in Sec. II C. Midrange CMF KWW$_1$ fits for four different x_c values of the present material, which include those values considered here and involve
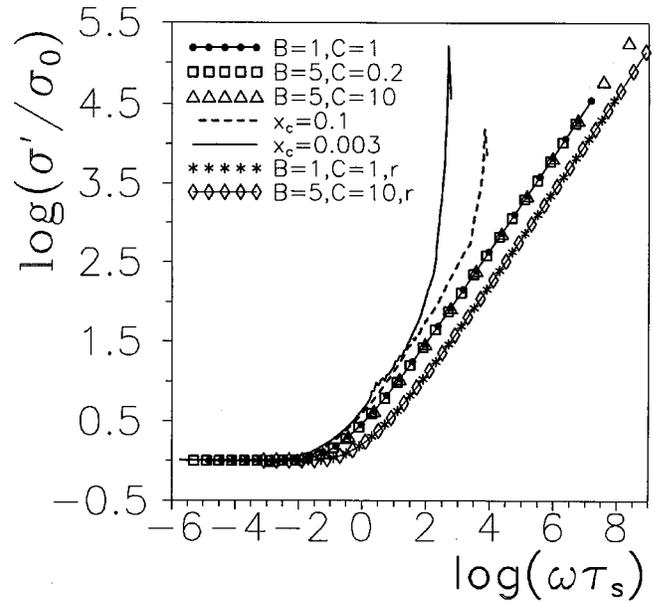
some temperature differences, all showed that β_1 was very nearly independent of both concentration and temperature in the ranges considered.[26]

Power-law fitting of the present $x_c=0.1$ $\sigma'(\omega)$ data above $\log(\sigma'/\sigma_0)\sim2.6$ yielded a surprising exponent estimate of about 1.3 for a limited frequency range. Current unpublished work of the author shows that a CPE response element in series with the bulk response may lead to added response beyond that of the bulk with a power-law exponent of $(2-\gamma_{SC})$ over a considerable range, a response that then approaches the basic SCPE exponent of γ_{SC}. Thus, the above large slope may possibly be explained as an electrode effect with $\gamma_{SC}\approx0.7$.

The two scaled synthetic data sets included in Fig. 9 are related to those of Fig. 1. Here, the parameter values used in generating the CMF KWW$_1$ data were $\beta_1=0.4$, $\varepsilon_{D\infty}=5$, $\rho_0=B\cdot A$, and $\tau_o=1.5\times10^{-5}C$ s, where the values of B and C employed are listed in Fig. 9. Further, $\tau_S=r\tau_o$, where $r=1$ for the left-most line and $r=5.43$ for the right one. Here, this value is the ratio between ε_{C10} and $\varepsilon_{C1\infty}$ for the present data. Thus, the left line involves scaling with $\varepsilon_{C1\infty}$ and the right one with ε_{C10}. It is evident that scaling works for both of these choices for r and it would, in fact, work for any other value of r.

Roling has pointed out that accurate scaling may not hold for a limited region near the knee of the $\sigma'(\omega)$ response where it is not much larger than σ_0.[4] He illustrated such behavior for $x_c=0.1-0.3$ values of x_c Na$_2$O$\cdot$(1$-x_c$) B$_2$O$_3$ glass which differed only by a factor of 3. Here, the two x_c values for the Sidebottom data[6] that we are using differ by a factor of about 33. Figure 10, which involves only a small range of σ'/σ_0, illustrates the effect for the original data.
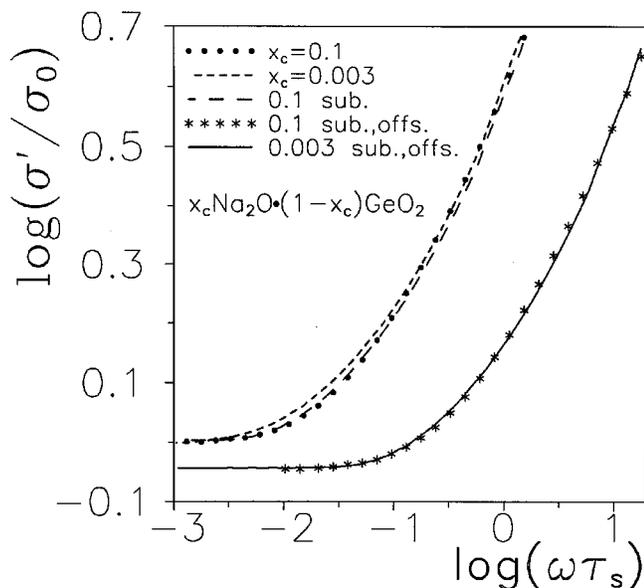
FIG. 10. $\sigma'(\omega)$ scaling results for the x_c Na$_2$O·$(1-x_c)$ GeO$_2$ data of Fig. 9 for response limited to that near the origin. Here, ''sub.'' indicates that the effects of extra series or parallel elements have been subtracted from the data, and ''off.'' specifies that curves have been offset for clarity.

Although the effect is evident, it is considerably smaller for these data than that presented by Roling, even though the mobile-ion concentration ratio is much larger here.

In addition to this comparison, we also show in Fig. 10 one between the two concentrations for data from which the added parallel- or series-element effects have been subtracted. The right curve and points, which have been offset in both axes for clarity, show that there remains no significant difference for such subtracted results. Evidently, the difference observed for raw data sets arises from that part of them associated with the extra fitting element needed to obtain a best fit and is not an inherent part of the bulk data themselves, that part which may usually be well fitted with a CMF KWW$_1$ model alone. If so, the Roling and co-worker[4,51] explanation for the effect as arising from mixed-alkali composition differences is inapplicable.

ACKNOWLEDGMENTS

[1] B. Roling, A. Happe, K. Funke, and M. D. Ingram, Phys. Rev. Lett. **78**, 2160 (1997).

[2] D. L. Sidebottom, P. F. Green, and R. K. Brow, Phys. Rev. B **56**, 170 (1997).

[3] K. L. Ngai and C. T. Moynihan, MRS Bull. **23**, 51 (1998).

[4] B. Roling, Solid State Ionics **105**, 185 (1999).

[5] B. Roling, J. Non-Cryst. Solids **244**, 34 (1999).

[6] D. L. Sidebottom, Phys. Rev. Lett. **82**, 3653 (1999).

[7] A. Ghosh and M. Sural, Europhys. Lett. **47**, 688 (1999).

[8] J. C. Dyre and T. B. Schrøder, Rev. Mod. Phys. **72**, 873 (2000).

[9] D. L. Sidebottom, B. Roling, and K. Funke, Phys. Rev. B **63**, 24301 (2001).

[10] W. C. Hasz, C. T. Moynihan, and P. A. Tick, J. Non-Cryst. Solids **172–174**, 1363 (1994).

[11] H. Jain and S. Krishnawami, Solid State Ionics **105**, 129 (1998).

[12] A. Pan and A. Ghosh, Phys. Rev. B **59**, 899 (1999).

[13] N. Zouari, H. Khemakhem, T. Mhiri, and A. Daoud, J. Phys. Chem. Solids **60**, 1779 (1999).

[14] M. Sural and A. Ghosh, Solid State Ionics **120**, 27 (1999).

[15] M. Sural and A. Ghosh, Solid State Ionics **126**, 315 (1999).

[16] M. Sural and A. Ghosh, Solid State Ionics **130**, 259 (2000).

[17] A. Pan and A. Ghosh, J. Chem. Phys. **112**, 1503 (2000).

[18] V. V. Shilov, V. V. Shevchenko, P. Pissis, A. Kryitsis, G. Georgoussis, Yu. P. Gomza, S. D. Nesin, and N. S. Klimenko, J. Non-Cryst. Solids **275**, 116 (2000).

[19] J. C. Dyre, J. Appl. Phys. **64**, 2456 (1988).

[20] J. R. Macdonald, J. Appl. Phys. **65**, 4845 (1989).

[21] J. R. Macdonald, Phys. Rev. B **49**, 9428 (1994).

[22] J. R. Macdonald, J. Non-Cryst. Solids **197**, 83 (1996); **204**, 309 (1996).

[23] J. R. Macdonald, J. Non-Cryst. Solids **212**, 95 (1997); **220**, 107 (1997).

[24] I. Svare, F. Borsa, D. R. Torgeson, S. W. Martin, and H. K. Patel, J. Non-Cryst. Solids **185**, 297 (1995).

[25] J. R. Macdonald, Solid State Ionics **133**, 79 (2000).

[26] J. R. Macdonald, Solid State Ionics (submitted).

[27] D. W. Davidson and R. H. Cole, J. Chem. Phys. **19**, 1417 (1951).

[28] V. Provenzano, L. P. Boesch, V. Volterra, C. T. Moynihan, and P. B. Macedo, J. Am. Ceram. Soc. **55**, 492 (1972).

[29] P. B. Macedo, C. T. Moynihan, and R. Bose, Phys. Chem. Glasses **13**, 171 (1972).

[30] C. T. Moynihan, L. P. Boesch, and N. L. Laberge, Phys. Chem. Glasses **14**, 122 (1973).

[31] R. Kohlrausch, Pogg. Ann. Phys. **91**, 179 (1854).

[32] G. Williams and D. C. Watts, Trans. Faraday Soc. **66**, 80 (1970).

[33] J. R. Macdonald and L. D. Potter, Jr., Solid State Ionics **23**, 61 (1987); J. R. Macdonald, J. Comput. Phys. **157**, 280 (2000); the newest version of the comprehensive LEVM fitting program may be downloaded at no cost from http://www.physics.unc.edu/~macd/; it includes an extensive manual, executable programs, and full source code. More information is provided about LEVM at this www address.

[34] V. O. Nguyen, J. S. Sanghera, I. K. Lloyd, I. D. Aggarwal, and D. Gershon, J. Non-Cryst. Solids **276**, 151 (2000).

[35] J. R. Macdonald, Phys. Rev. B 52205 (2001).

[36] H. Scher and M. Lax, Phys. Rev. B **7**, 4491 (1973).

[37] C. P. Lindsey and G. D. Patterson, J. Chem. Phys. **73**, 3348 (1980).

[38] T. B. Schrøder and J. C. Dyre, Phys. Rev. Lett. **84**, 310 (2000).

[39] B. Roling, C. Martiny, and K. Funke, J. Non-Cryst. Solids **249**, 201 (1999).

[40] K. L. Ngai and R. W. Rendell, Phys. Rev. B **61**, 9393 (2000).

[41] C. León, P. Lunkenheimer, and K. L. Ngai, Phys. Rev. B. (submitted).

[42] D. L. Sidebottom, P. F. Green, and R. K. Brow, J. Non-Cryst. Solids **183**, 151 (1995).

[43] H. Namikawa, J. Non-Cryst. Solids **18**, 173 (1975).

[44] K. L. Ngai and C. León, Phys. Rev. B **60**, 9396 (1999).

[45] J. R. Macdonald, J. Appl. Phys. **82**, 3962 (1997).

[46] C. T. Moynihan, J. Non-Cryst. Solids **172-174**, 1395 (1994); **203**, 359 (1996).

[47] *Impedance Spectroscopy – Emphasizing Solid Materials and Systems,* edited by J. R. Macdonald (Wiley-Interscience, New York, 1987).

[48] A. S. Nowick and B. S. Lim, J. Non-Cryst. Solids **172-174**, 1389 (1994).

[49] J. R. Macdonald, Appl. Phys. A: Solids Surf. **59**, 181 (1994).

[50] J. R. Macdonald, J. Non-Cryst. Solids **210**, 70 (1997).

[51] B. Roling, A. Hoppe, M. D. Ingram, and K. Funke, J. Phys. Chem. B **103**, 4122 (1999).